A Multi-Agent FLISR Model for Safety-Critical Smart Grids

Chaudhry Talha Hassan, Muhammad Shamaas, Tariq Mahmood Jadoon

Department of Electrical Engineering, Lahore University of Management Sciences, Lahore 54792, Pakistan

chaudhry.hassan@lums.edu.pk, muhammad.shamaas@lums.edu.pk, jadoon@lums.edu.pk

Abstract –*Resilient smart grids must guarantee fast service restoration during unexpected faults and natural disasters. This can be achieved by isolating the faults and forming microgrids around black-start generators. A self-sufficient microgrid must achieve service restoration through optimal control of distributed generators and energy storage systems. The reconfiguration of the distribution system can be achieved by solving the restoration optimization problem. However, the implementation of the optimal solution may be infeasible if the unpredictable transient response triggers the electrical protection system. It is important that the transient results of electrical power flow must be used to enforce dynamic stability after every restoration stage. In this research, measurements from distributed phasor measurement units are used to quantify the disturbance experienced by the loads, generators, and lines. This feedback is used to restrain the restoration algorithm so that the microgrid gets sufficient time to stabilize. Decentralized control is implemented to solve the serious challenges of information discovery, real-time task scheduling, communication network congestion, and big data analysis. The importance of multi-agent coordination for power system dynamic stability is analyzed by simulating network congestion of control and metering systems. The approach is validated over a modified IEEE-123 node test feeder, and the results are presented to demonstrate the efficacy of the framework for multiple fault scenarios*.

Keywords: Energy storage system (ESS), inverter-based distributed generator (IBDG), mixed-integer second-order cone programming (MISOCP), wide-area situational awareness (WASA).

NOMENCLATURE

Sets

Ω_{BK}	Set of bus blocks.
Ω_{BS}	Set of generators with black start capability.
Ω_{G}	Set of generators.
Ω_{IBDG}	Set of inverter-based generators.
Ω_{L}	Set of distribution lines.
Ω_{NBS}	Set of generators without black start capability.
Ω_{NSW}	Set of non-switchable lines.
Ω_{φ}	Set of phases.
Ω_{SG}	Set of synchronous generators.
Ω_{SW}	Set of switchable lines.
Ω_{Z}	Set of loads.

Indices

bk	Index of bus block.
g	Index of generator.
i, j	Index of bus.
k, l	Index of distribution line.
m	Index of microgrid.
φ	Index of phase.
t	Index of time step.
z	Index of load.

Parameters

α	Multiplier for dynamic stability factor equation.
B_{ij}	Imaginary part of transmission line admittance.
D	Load damping rate
D_P	P-ω and Q-V droop gains.
f_0	Nominal steady state frequency.
f_{max}	Maximum allowable frequency limit.
f_{min}	Minimum allowable frequency limit.
G_{ij}	Real part of transmission line admittance.
H	System inertia.
$I_{l,max}^{line}$	Maximum phase current limit of distribution line l.
I_{θ}	Power factor angle of constant current load.
$J_{i,j}$	$i \times j$ matrix of ones.
M	Big-M number.
$P_{l,\varphi}^{line}$	3×3 phase matrix of line l.
$P_{g,max}^{gen}$	Maximum output real power limit of generator g.
$P_{l,max}^{line}$	Maximum output real power limit of distribution line l.
P_{θ}	Power factor angle of constant power load.
PLF_{l}^{line}	Line loss factor for active power.
$Q_{g,max}^{gen}$	Maximum output reactive power limit of generator g.
$Q_{l,max}^{line}$	Maximum output reactive power limit of distribution line l.
QLF_{l}^{line}	Line loss factor for reactive power.
R_{l}	3×3 resistance matrix of line l.
$S_{l,max}^{line}$	Maximum output apparent power limit of distribution line l.
$S_{b,max}^{ESS}$	Maximum input apparent power limit of ESS b.
$S_{g,max}^{gen}$	Maximum output apparent power limit of generator g.
S_{n}	Nominal apparent power rating of ZIP load.
$SOC_{b,max}^{ESS}$	Maximum limit of SOC for ESS b.
$SOC_{b,min}^{ESS}$	Minimum limit of SOC for ESS b.
T	Length of rolling horizon.
$U_{i,max}^{bus}$	Maximum squared voltage magnitude limit of bus i.
$U_{i,min}^{bus}$	Minimum squared voltage magnitude limit of bus i.

V_0 Nominal phase to ground rms bus voltage.
w_i^{load} Priority weight for load of bus i.
X_l 3×3 Reactance matrix of line l.
Z_l 3×3 Impedance matrix of line l.
Z_θ Power factor angle of constant impedance load.
Δf^{max} Limit for maximum allowable frequency deviation.
Δf^{meas} Measured maximum transient frequency deviation.
ΔI^{max} Limit for maximum allowable current deviation.
ΔI^{meas} Measured maximum transient current deviation.
ΔV^{max} Limit for maximum allowable voltage deviation.
ΔV^{meas} Measured maximum transient voltage deviation.
Δt Time step between two restoration stages.
η_b^{ESS} Charging efficiency of ESS b.

Variables

$DF_{m,t}$ Disturbance factor of microgrid m at stage t.
P_i^{bus} Real power injection at bus i.
$P_{b,\varphi,t}^{ESS}$ Active power output of ESS b, phase φ at stage t.
$P_{m,t}^{res}$ Limit of maximum restored load for microgrid m at stage t.
$P_{l,\varphi,t}^{line}$ Active power flow of line l, phase φ at stage t.
$P_{l,\varphi,t}^{lineloss}$ Active power loss of line l, phase φ at stage t.
$P_{g,\varphi,t}^{gen}$ Active power output of generator g, phase φ at stage t.
$P_{z,\varphi,t}^{load}$ Active power demand of load z, phase φ at stage t.
Q_i^{bus} Reactive power injection at bus i.
$Q_{b,\varphi,t}^{ESS}$ Reactive power output of ESS b, phase φ at stage t.
$Q_{l,\varphi,t}^{line}$ Reactive power flow of line l, phase φ at stage t.
$Q_{l,\varphi,t}^{lineloss}$ Reactive power loss of line l, phase φ at stage t.
$Q_{g,\varphi,t}^{gen}$ Reactive power output of generator g, phase φ at stage t.
$Q_{z,\varphi,t}^{load}$ Reactive power demand of load z, phase φ at stage t.
$SOC_{b,\varphi,t}^{ESS}$ SOC of ESS b, phase φ at stage t.
$U_{i,t}^{bus}$ 3×1 squared three-phase voltage magnitude matrix of bus i at stage t.
$V_{i,t}^{bus}$ Phase to ground rms voltage of bus i at stage t.
$x_{i,t}^{bus}$ Binary energization status of bus i.
$x_{bk,t}^{busblock}$ Binary energization status of bus block bk.
$x_{b,t}^{charge}$ Binary charging status of ESS b.
$x_{g,t}^{gen}$ Binary energization status of generator g.
$x_{l,t}^{line}$ Binary energization status of line l.
$x_{z,t}^{load}$ Binary energization status of load l.
ΔP_{IBDG} Increased output from inverter-based generators.
ΔP_L Total generation loss.
$\Delta P_{m,t}^{res}$ Maximum limit for restored load of microgrid m at stage t.
ΔP_{SG} Increased output from synchronous generators.
θ_i^{bus} Angle of voltage at bus i.

I. INTRODUCTION

Modern smart grids with distributed generation must guarantee high reliability of service to consumers. Although faults are inevitable, uninterruptible service must be ensured for critical loads. During an unexpected emergency, the generation capacity and energy reserves must be carefully utilized to recover critical loads. An effective method for emergency service restoration is the sectionalization of the power network into microgrids [1]. These autonomous units coordinate all the decisions for self-healing. Hence, power restoration can be achieved in a decentralized manner.

Microgrid restoration can be very challenging for inverter-dominated smart grids because these networks suffer from poor dynamic stability [1]. Operating multiple inverter-based generators can be difficult if they have dissimilar droop characteristics and ramp limitations. The unpredictable nature of non-linear semiconductor devices makes inverters especially susceptible to damage during electrical overloads, voltage fluctuations, and short-circuit faults [2]. Inverters can face commutation failure or permanent damage if the maximum limits for safe operation are breached. Optimal power exchange must be ensured to prevent the overstressing of IBDGs.

The implementation of the optimal power flow solution can present serious challenges during information discovery, real-time task scheduling, communication network congestion and big data analysis [3]. Perfect coordination must be maintained between the microgrid controller, distributed generators and smart switches to prevent microgrid instability.

The distributed control system has to schedule multiple hard real time tasks for execution of the optimal solution. It must also ensure that each real time task has reasonable delay, duration and deadline constraints [4]. Centralized control is not a viable option for this safety-critical system [5]. A multi-agent control scheme must be developed to facilitate information discovery, real-time task scheduling, communication network load balancing and big data analysis [6] [7] [2].

Reconfiguration of an inverter-dominated distribution system is a complex combinatorial problem due to non-linear power flow equations and the unpredictable generation of renewable energy sources [2]. A highly complicated optimization scheme is needed to incorporate all the intricacies of the analog and digital components. The optimization model can only approximate the electrical power network equations. Hence, the results of electrical power flow must be used to reinforce dynamic stability after every restoration stage [1].

An intelligent control system must be well informed about the situation of all the constituent subsystems. The control commands must be based on real-time data obtained from distributed field devices [4]. In short, an active management system is needed to sense and optimally control all the distributed subsystems. The proposed fault location and service restoration (FLISR) model [8] is shown in Figure 1.

This research aims to achieve the following goals:

1. Develop a decentralized multi-agent system architecture for the restoration of inverter-dominated microgrids [2] [3]. The microgrid restoration was based on the prior information of distributed generators, distribution network configuration, and load demand forecast [4]. The microgrid controller performed MISOCP optimization for controlling distributed generators, demand response, and network reconfiguration. Based on the restoration solution, it distributed control commands to the different smart switches and bus block controllers. Hence, these autonomous controllers were responsible for coordinating the operation of distributed loads, switches and generators.

2. Execute information exchange to coordinate the control and protection of microgrids during sequential service

restoration [6] [2]. The microgrid controller was responsible for monitoring all the widespread loads, lines and generators. It aggregated the status information and distributed the control commands for all the subsystems [3] [4]. The hierarchical structure for data exchange was implemented using a fast and reliable communication system in NS-3 [9].

3. Quantify the aggression afflicted during each microgrid restoration stage to provide feedback for the microgrid protection system [1]. After every restoration stage, the transient fault records of the GridLAB-D [7] simulation were analyzed to quantify the disturbance experienced by the microgrid. The maximum deviations in load voltages, line currents, and generator frequencies were used to calculate the microgrid disturbance factor. A rolling horizon optimization framework was implemented to modulate the load restoration limit based on the microgrid disturbance factor. This factor restrained the sequential restoration algorithm so that the next stage could be improved.

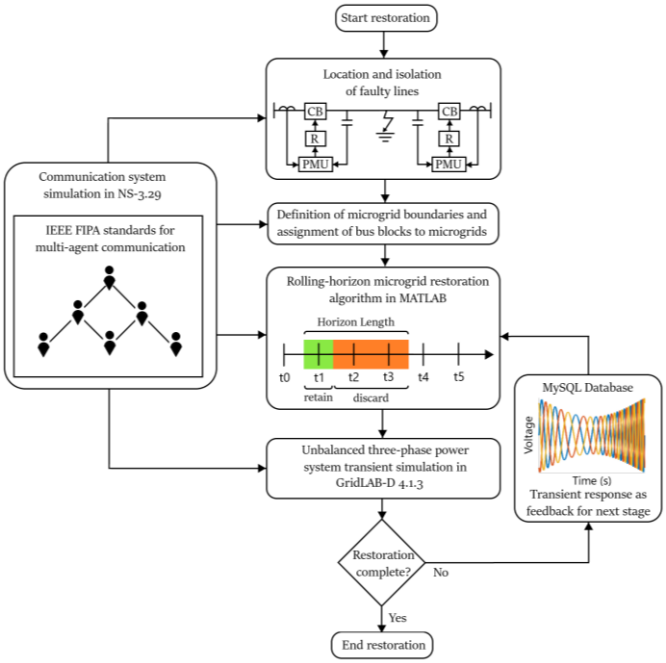

Figure 1: FLISR model for smart grid.

II. Formulation Of Optimization Problem

A MISOCP optimization problem was formulated for the restoration of the damaged IEEE-123 bus system [10] shown in Figure 2. The modified network contained three-phase diesel generators, PV generators, and EV charging stations. Each generator had a rating of 1 MVA and a ramp limit of 150 kW/s.

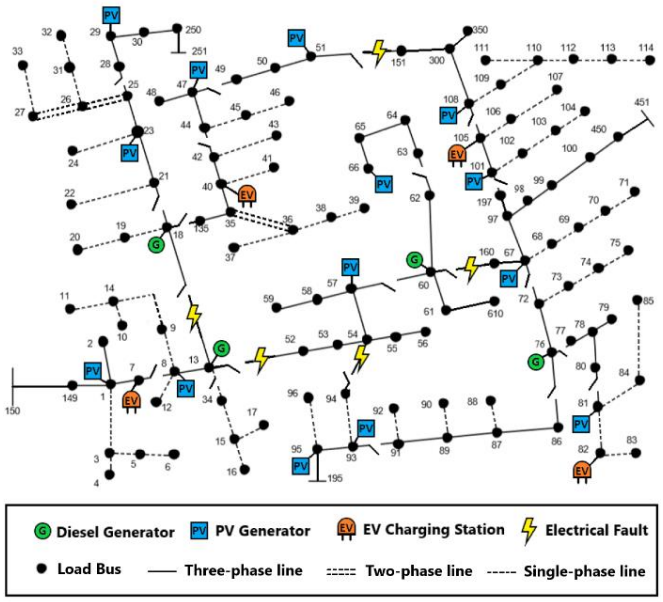

Figure 2: Damaged IEEE 123 bus distribution network.

The service restoration system executed a self-healing algorithm. The initial decision for network reconfiguration was based on the fault location input. The unhealthy region was isolated immediately. Afterward, iterative microgrid formation started.

The objective function (1) aims to maximize the total recovered loads over a rolling horizon $[t, t+T]$. The priorities of the bus blocks were assigned randomly. Each load had the same weight as its bus block.

$$\max \sum_{t\epsilon[t,t+T]} \sum_{z\epsilon\Omega_Z} \sum_{\varphi\epsilon\Omega_\varphi} (T-t) \times \left(w_z^{load} x_{z,t}^{load} P_{z,\varphi,t}^{load}\right) \quad (1)$$

1. Nodal power balance constraints: Constraints (2)-(3) define the nodal balance of active and reactive power for each phase. The linearized DistFlow equations were used to approximate the electrical power flow. They state that the generated power must be equal to the sum of load demand, transmitted power, and line losses.

$$\forall i \forall \varphi \forall t \left[\sum_{l\epsilon\Omega_i} \left(P_{l,\varphi,t}^{line} + P_{l,\varphi,t}^{lineloss}\right) + x_{i,t}^{load} P_{i,\varphi,t}^{load} - P_{i,\varphi,t}^{ESS} = P_{i,\varphi,t}^{gen}\right] \quad (2)$$

$$\forall i \forall \varphi \forall t \left[\sum_{l\epsilon\Omega_i} \left(Q_{l,\varphi,t}^{line} + Q_{l,\varphi,t}^{lineloss}\right) + x_{i,t}^{load} Q_{i,\varphi,t}^{load} - Q_{i,\varphi,t}^{ESS} = Q_{i,\varphi,t}^{gen}\right] \quad (3)$$

2. Transmission line constraints: Constraints (4)-(7) define the limits for transmission line active power losses and reactive power losses. The line losses were calculated using the average loss factor and the apparent power flow of the line. The line loss factor was estimated by assuming a maximum voltage drop of 5% across the line [5].

$$PLF_l^{line} \approx \frac{P_{l,max}^{lineloss}}{S_{l,max}^{line}} = \frac{R_l I_{l,max}^{line\,2}}{V_0 I_{l,max}^{line}} = \frac{0.05 R_l}{\sqrt{R_l^2 + X_l^2}};\ I_{l,max}^{line} \approx \frac{0.05 V_0}{\sqrt{R_l^2 + X_l^2}} \quad (4)$$

$$QLF_l^{line} \approx \frac{Q_{l,max}^{lineloss}}{S_{l,max}^{line}} = \frac{X_l I_{l,max}^{line\,2}}{V_0 I_{l,max}^{line}} = \frac{0.05 X_l}{\sqrt{R_l^2 + X_l^2}};\ I_{l,max}^{line} \approx \frac{0.05 V_0}{\sqrt{R_l^2 + X_l^2}} \quad (5)$$

$$\forall l\epsilon\Omega_L \forall t \left[P_{l,t}^{lineloss} \geq PLF_l^{line} \left\| \begin{matrix} P_{l,\varphi,t}^{line} \\ Q_{l,\varphi,t}^{line} \end{matrix} \right\|_2\right] \quad (6)$$

$$\forall l \epsilon \Omega_L \forall t \left[Q_{l,t}^{lineloss} \geq QLF_l^{line} \left\| \begin{matrix} P_{l,\varphi,t}^{line} \\ Q_{l,\varphi,t}^{line} \end{matrix} \right\|_2 \right] \quad (7)$$

Constraint (8) defines the transmission line's active and reactive power flow limits. Constraints (9)-(10) state the conditions for the energization of switchable lines. Constraint (11) implies that non-switchable lines are automatically energized whenever the corresponding bus is energized.

$$\forall l \forall \varphi \forall t \left[\left\| \begin{matrix} P_{l,\varphi,t}^{line} \\ Q_{l,\varphi,t}^{line} \end{matrix} \right\|_2 \leq x_{l,t}^{line} S_{l,max}^{line} \right] \quad (8)$$

$$\forall ij, l \epsilon \Omega_{SW} \forall t \left[x_{l,t}^{line} \leq x_{i,t}^{bus} \wedge x_{l,t}^{line} \leq x_{j,t}^{bus} \right] \quad (9)$$

$$\forall ij, l \epsilon \Omega_{SW} \forall t \epsilon [2, \infty) \left[x_{l,t}^{line} \geq x_{l,t-1}^{line} \right] \quad (10)$$

$$\forall ij, l \epsilon \Omega_{NSW} \forall t \left[x_{l,t}^{line} = x_{i,t}^{bus} \wedge x_{l,t}^{line} = x_{j,t}^{bus} \right] \quad (11)$$

3. Generation constraints: Constraints (12)-(13) define the active and reactive power generation limits for generators. Constraints (14)-(18) define the operational limits for charging and discharging of energy storage systems [6] [5]. Constraints (19)–(20) state that a generator without black start capability can only be started if its associated bus is energized, and it cannot be turned off afterwards. Constraints (21)-(22) define the output active and reactive power ramp rates for the distributed generators (PV inverters, PHEV inverters, and diesel generators) [2] [4].

$$\forall g \forall \varphi \forall t \left[\left\| \begin{matrix} P_{g,\varphi,t}^{gen} \\ Q_{g,\varphi,t}^{gen} \end{matrix} \right\|_2 \leq x_{g,t}^{gen} S_{g,max}^{gen} \right] \quad (12)$$

$$\forall g \forall \varphi \forall t \left[P_{g,\varphi,t}^{gen} \geq 0 \wedge Q_{g,\varphi,t}^{gen} \geq 0 \right] \quad (13)$$

$$\forall b \forall \varphi \forall t \left[\left\| \begin{matrix} P_{b,\varphi,t}^{ESS} \\ Q_{b,\varphi,t}^{ESS} \end{matrix} \right\|_2 \leq x_{b,t}^{charge} S_{b,max}^{ESS} \right] \quad (14)$$

$$\forall g \forall \varphi \forall t [x_{g,t}^{charge} + x_{g,t}^{gen} = 1] \quad (15)$$

$$\forall b \forall \varphi \forall t \left[P_{b,\varphi,t}^{ESS} \leq 0 \wedge Q_{b,\varphi,t}^{ESS} \leq 0 \right] \quad (16)$$

$$\forall b \forall \varphi \forall t \left[SOC_{b,\varphi,t}^{ESS} \geq SOC_{b,min}^{ESS} \wedge SOC_{b,\varphi,t}^{ESS} \leq SOC_{b,max}^{ESS} \right] \quad (17)$$

$$\forall b \forall \varphi \forall t \left[SOC_{b,\varphi,t}^{ESS} = SOC_{b,\varphi,t-1}^{ESS} - \eta_b^{ESS} \Delta t \left(P_{b,\varphi,t}^{ESS} + P_{b,\varphi,t}^{gen} + Q_{b,\varphi,t}^{ESS} + Q_{b,\varphi,t}^{gen} \right) \right] \quad (18)$$

$$\forall g \epsilon \Omega_{NBS} \forall t \left[x_{g,t}^{gen} \leq x_{g,t}^{bus} \right] \quad (19)$$

$$\forall g \epsilon \Omega_{NBS} \forall t \epsilon [2, \infty) \left[x_{g,t}^{gen} \geq x_{g,t-1}^{gen} \right] \quad (20)$$

$$\forall g \forall t \epsilon [2, \infty) \left[-\Delta P_{g,max}^{gen} \leq P_{g,t}^{gen} - P_{g,t-1}^{gen} \leq \Delta P_{g,max}^{gen} \right] \quad (21)$$

$$\forall g \forall t \epsilon [2, \infty) \left[-\Delta Q_{g,max}^{gen} \leq Q_{g,t}^{gen} - Q_{g,t-1}^{gen} \leq \Delta Q_{g,max}^{gen} \right] \quad (22)$$

4. Load constraints: Constraint (23) states that a load is energized whenever its corresponding bus has been energized. Constraint (24) states that once a load has started operation, it cannot be stopped.

$$\forall i \forall t \left[x_{i,t}^{load} = x_{i,t}^{bus} \right] \quad (23)$$

$$\forall i \forall t \epsilon [2, \infty) \left[x_{i,t}^{load} \geq x_{i,t-1}^{load} \right] \quad (24)$$

5. Nodal voltage constraints: Constraints (25)-(26) define the limits for the voltage difference between the end nodes of a transmission line. The Big-M notation is used to ensure that these constraints are active only when the line is energized. Constraint (27) ensures that the bus voltage is constrained within predefined limits.

$$\forall ij, l \epsilon \Omega_L \forall \varphi \forall t \left[U_{i,\varphi,t}^{bus} - U_{j,\varphi,t}^{bus} \geq 2 \left(R_l P_{l,\varphi,t}^{line} + X_l Q_{l,\varphi,t}^{line} \right) + \left(x_{l,t}^{line} + P_{l,\varphi}^{line} - 2 \right) M \right] \quad (25)$$

$$\forall ij, l \epsilon \Omega_L \forall \varphi \forall t \left[U_{i,\varphi,t}^{bus} - U_{j,\varphi,t}^{bus} \leq 2 \left(R_l P_{l,\varphi,t}^{line} + X_l Q_{l,\varphi,t}^{line} \right) + \left(2 - x_{l,t}^{line} - P_{l,\varphi}^{line} \right) M \right] \quad (26)$$

$$\forall i \forall \varphi \forall t \left[x_{i,t} U_{i,min}^{bus} \leq U_{i,\varphi,t}^{bus} \leq x_{i,t} U_{i,max}^{bus} \right] \quad (27)$$

6. Bus block switching: The healthy bus blocks were enumerated and grouped based on geographic proximity. The reduced network contained a set of bus blocks Ω_{BK} that were connected by a set of switchable lines:

$$\Omega_{SW} \coloneqq \{(k, l) \mid k \epsilon \Omega_{BK} \wedge l \epsilon \Omega_{BK} \wedge k \neq l\} \quad (28)$$

The reduced IEEE-123 bus system is shown in Figure 3. Constraint (29) ensures that all the buses in a bus block get energized simultaneously. Constraint (30) ensures that a switchable line cannot be closed if both of its end blocks are already energized. This is required to maintain radial tree topology during microgrid restoration. Constraint (31) states that a bus block can only be switched on by one of the connected switchable lines. Constraint (32) makes sure that at least one connected switchable line is energized before the energization of the bus block. Finally, constraint (33) implies that a switchable line can be energized only if at least one of the connected bus blocks is already energized.

$$\forall i \epsilon \Omega_{bk} \forall t \left[x_{i,t}^{bus} = x_{bk,t}^{busblock} \right] \quad (29)$$

$$\forall k, ij \epsilon \Omega_{sw} \forall t \epsilon [2, \infty) \left[\left(x_{i,t}^{busblock} - x_{i,t-1}^{busblock} \right) + \left(x_{j,t}^{busblock} - x_{j,t-1}^{busblock} \right) \geq \left(x_{k,t}^{line} - x_{k,t-1}^{line} \right) \right] \quad (30)$$

$$\forall k, ij \epsilon \Omega_{sw} \forall t \epsilon [2, \infty) \left[\sum_{ki \epsilon \Omega_{sw}} \left(P_{ki,\varphi,t}^{line} - P_{ki,\varphi,t-1}^{line} \right) + \sum_{ij \epsilon \Omega_{sw}} \left(P_{ij,\varphi,t}^{line} - P_{ij,\varphi,t-1}^{line} \right) \leq 1 + x_{i,t-1}^{busblock} M \right] \quad (31)$$

$$\forall k, ij \epsilon \Omega_{sw} \forall t \epsilon [2, \infty) \left[x_{i,t-1}^{busblock} \leq \sum_{ki \epsilon \Omega_i} x_{ki,t}^{line} + \sum_{ij \epsilon \Omega_i} x_{ij,t}^{line} \right] \quad (32)$$

$$\forall k, ij \epsilon \Omega_{sw} \forall t \epsilon [2, \infty) \left[x_{ij,t}^{line} \leq x_{i,t-1}^{busblock} + x_{j,t-1}^{busblock} \right] \quad (33)$$

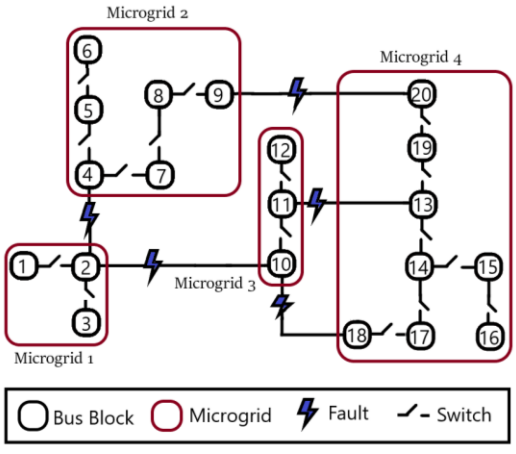

Figure 3: Reduced IEEE-123 bus power network showing bus blocks and microgrids.

7. Dynamic constraints: After a restoration stage was executed, the maximum values for generator frequency deviation, active power deviation, and reactive power deviation were recorded. These values were translated into a numerical parameter for expressing the state of the microgrid [1]. Equation (34) presents the formula for calculating this microgrid disturbance factor. This factor was used to restrain the amount of restored load in the next stage, as expressed in

(35)-(36). The maximum power deviation of each phase was incorporated to discourage unbalanced loading of generators.

$$DF_{m,t} = \frac{1}{7}\left[\sum_{g\epsilon\Omega_m}\frac{1}{N_i}\left(\frac{\Delta f_{g,t}^{meas}}{f^{base}} + \frac{\Delta V_{g,\varphi_A,t}^{meas}+\Delta V_{g,\varphi_B,t}^{meas}+\Delta V_{g,\varphi_C,t}^{meas}}{V^{base}} + \frac{\Delta S_{g,\varphi_A,t}^{meas}+\Delta S_{g,\varphi_B,t}^{meas}+\Delta S_{g,\varphi_C,t}^{meas}}{S^{base}}\right)\right] \quad (34)$$

$$\forall m \forall t \epsilon [2,\infty)[\Delta P_{m,t}^{res} = \Delta P_{m,t-1}^{res} + \alpha(1 - DF_{m,t-1})] \quad (35)$$

$$\forall m \forall t \epsilon [2,\infty)[0 \le P_{m,t}^{res} \le P_{m,t-1}^{res} + \Delta P_{m,t}^{res}] \quad (36)$$

III. Multi-agent Coordination Model

The implementation of the optimal power flow solution can present serious challenges during information discovery, real-time task scheduling, communication network congestion and big data analysis [3]. Perfect coordination must be maintained between the microgrid controller, distributed generators and smart switches to prevent microgrid instability.

The distributed control system has to schedule multiple hard real time tasks for execution of the optimal solution. It must also ensure that each real time task has reasonable delay, duration and deadline constraints. Centralized control is not a viable option for this safety-critical system [5]. A multi-agent control scheme was developed to facilitate information discovery, real-time task scheduling, communication network load balancing and big data analysis [3] [4]. The complete multi-agent system for a microgrid team is shown in Figure 4. Each microgrid was divided into several bus block teams headed by bus block master agents. Switch agents were responsible for connecting bus blocks together. Switch agents and bus block agents were controlled by the microgrid controller [6] [7] [2].

IEEE FIPA standard was used to build a unified model for the communication of reactive agents. Agent Communication Language (ACL) was used to transmit information signals between agents [6] [7]. A simple example of a microgrid with two bus blocks is shown in Figure 5. The stimulus event of unexpected generator fault triggered the multi-agent system FLISR sequence [8] [3]. The unhealthy bus block was isolated by requesting the switch agent to open the connecting switch.

After the isolation of the fault, the microgrid agent sent team proposals to the bus block and switch agents within its boundary. The agent that could join the microgrid accepted the proposal. After this handshake, the bus block agent proceeded to build its own team of load and generator agents.

The microgrid agent solved the MISOCP optimization problem and sent the control commands to the bus block team leader. The bus block agent informed all the bus block team members about the upcoming switching action. After confirming with the bus block agents, the microgrid agent commanded the switch agent to close, and the bus block got connected to the microgrid.

Later, the microgrid agent inquired the bus block agent about its status. The bus block made sure that every team member was operating in a safe and reliable manner. Then, it sent the aggregated information to the microgrid agent as response.

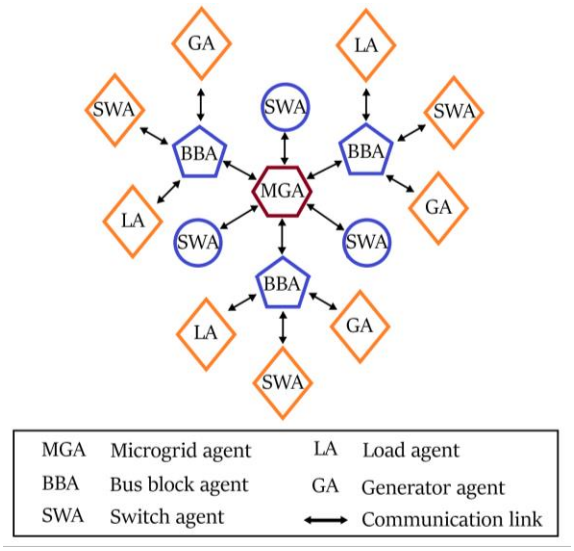

Figure 4: Multi-agent system for a microgrid.

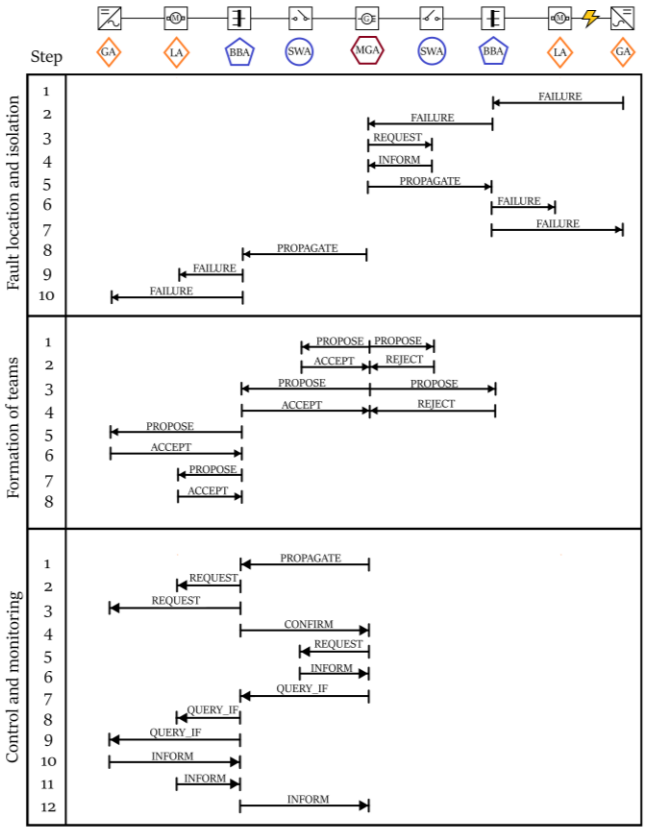

Figure 5: Multi-agent communication scheme for FLISR.

IV. Communication System

A three-level communication network was designed in NS-3 to enable the coordination between the microgrid controllers and bus block controllers [9]. Control signals were transmitted through the control system, whereas the metering data was transmitted through the monitoring system. Intelligent Electronic Devices (IEDs) installed in the field provided feedback for the reliable control of distributed generators, loads and smart switches [7] [4]. The complete communication system is shown in Figure 6.

A. Monitoring System

The AMI system was made up of smart meters, communication modules, data concentrators, and Meter Data Management System (MDMS). MDMS managed data storage to provide the information in a useful form to the microgrid controller. The IEEE C37.118 synchronized phasor measurement units (PMUs) reported the magnitude and phase angle of electrical voltage and current using a common time source for synchronization.

The Wide Area Network (WAN) provided remote access of bus blocks to the microgrid controller via long-range, high-capacity WiMAX links. NS-3 provided a realistic implementation of the IEEE-802.16 standard using wireless MAN-OFDM physical layer, uplink and downlink schedulers, IP packet classifier for the convergence sub-layer, and support for multicast traffic [9]. A base station was installed to serve the subscriber stations installed at the microgrid controller and the bus block controller nodes. The point-to-multipoint telecommunication network enabled pervasive control of the entire distribution system for time-sensitive tasks like maintaining electrical stability.

Existing power lines were used to transmit control and status signals across the Field Area Network (FAN). 2 Mbps links were used for power line carrier communication [9]. Each power line communication device was supplemented with a data concentrator for communication with the widespread IEDs [7] [3]. Distributed generators were controlled via programmable logic controllers integrated with SCADA modems. The transmission line channels also conveyed switching commands for capacitor banks, load controllers, and circuit breakers.

The Home Area Network (HAN) connected load controllers and sensors via an Ethernet-based AMI. This enabled coordination of a large number of distributed IEDs. These devices continuously collected information from power meters, transducers, and field components for supervision. 100 Mbps Ethernet links were installed for the Home Area Network. For fast and reliable communication, the IPv4 protocol was implemented in the network layer, and the UDP protocol was implemented in the transport layer [3] [7] [9]. The network interface module implemented distributed network protocols for physical interface conversion. The pervasive communication system enabled continuous scanning of operational data for greater control and flexibility.

B. Control System

The microgrid controller distributed command signals using high priority control packets. It was crucial to transmit control signals reliably with very low latency [3]. Control signal channels were designed to have low bandwidth but very high reliability (> 99 %). The maximum constraint for control packet latency was 20 ms.

The priority associated with a socket was used to determine the value of the Differentiated Services field (RFC 2474) of the IPv4 header. This is how DSCP values mapped onto priority values of the packets sent through that socket. DSCP CS6 (RFC 4594) was assigned for high priority network control packets. The packet priority was used by queueing disciplines to classify packets into distinct FIFO queues.

The microgrid agent was connected to the bus block agents using wireless LTE links in NS-3. The microgrid controller was connected to bus block UE through eNB, SGW and PGW nodes. The 3GPP specified S5 protocol stack, S1-U protocol stack and LTE radio protocol stack were simulated in LTE-EPC data plane. S1-MME, S11, S5 and X2 interface was modeled for the LTE-EPC control plane [9].

OpenFlow switch was installed in each bus block to connect bus block agent with the generator, switch and load agents. OpenFlow switch provides the programmability and flexibility required for smart grid architectures with ever-increasing demand. It provides support for traffic engineering and virtual private networks. These features are vital to enhance the reliability and scalability of the smart grid [9].

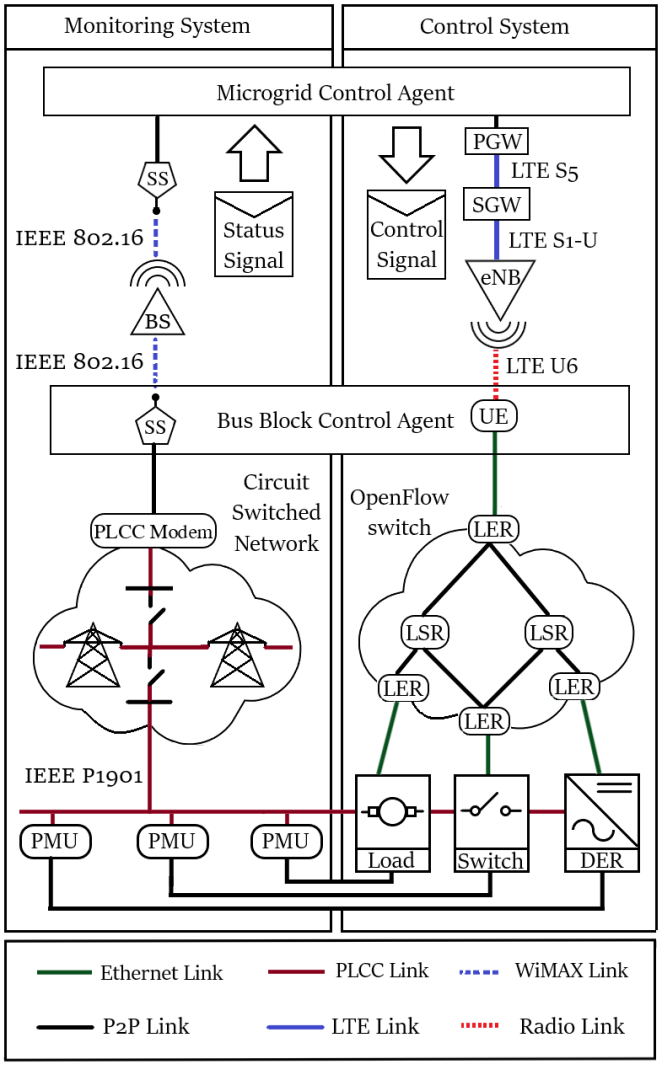

Figure 6: Communication system for monitoring and control signals.

V. Simulation Results

The simulation of the cyber-physical smart grid was carried out in three steps. First, the MISOCP optimization problem was solved to determine the optimal switching and control commands. Then, the NS-3 communication system simulation was run to determine the delays in the transmission of information to different subsystems. Finally, the outputs from the previous two simulations were implemented in the

GridLAB-D simulator to determine the power system transient response [7].

Three different cases were studied to analyze the efficacy of the proposed dynamic feedback system [1] in improving microgrid restoration.

A. Case 1: Ideal multi-agent communication.

The first case had ideal multi-agent coordination and resulted in the most stable restoration scheme. The frequency of grid-forming diesel generators is shown in Figure 7.

The restoration of microgrid 1 completed in three stages and involved 1128 messages. The timeline of the three stages of restoration is given below:

1. IBDG 8 ramped up to 815.4 kW. At 0.776 s, bus block 2 was energized by closing the circuit breakers of diesel generator 13 and IBDG 8.
2. IBDG 1, 7 and 8 were ramped up to 245.5 kW, 243.5 kW and 617.4 kW respectively. At 2.414 s, bus block 1 was energized by closing the circuit breaker of line 7-8.
3. IBDG 1, 7 and 8 were ramped up to 342.6 kW, 346.9 kW and 577.0 kW respectively. At 3.585 s, circuit breaker of line 13-34 was closed to energize bus block 3.

The restoration of microgrid 2 completed in four stages and involved 2658 messages. The timeline of the four stages of restoration is given below:

1. IBDG 23 and 40 ramped up to 604.8 kW and 858.6 kW respectively. Bus blocks 4, 5 and 7 were energized at 0.326 s, 1.630 s and 2.712 s respectively.
2. IBDG 23, 29 and 40 ramped up to 659.2 kW, 119.9 kW and 669.4 kW respectively. At 5.116 s, bus block 6 was energized by closing circuit breaker of line 25-28.
3. IBDG 23, 29, 40 and 47 ramped up to 633.9 kW, 249.6 kW, 715.7 kW and 138.4 kW respectively. At 6.153 s, bus block 8 was energized by closing circuit breaker of line 42-44.
4. IBDG 23, 29, 40, 47 and 51 ramped up to 636.8 kW, 356.5 kW, 729.0 kW, 281.6 kW and 131.2 kW. At 7.153 s, bus block 9 was energized by closing the circuit breaker of line 47-49.

The restoration of microgrid 3 completed in three stages and involved 888 messages. The timeline of the three stages of restoration is given below:

1. At 0.306 s, bus block 11 was energized by closing the circuit breaker of diesel generator 60.
2. IBDG 57 ramped up to 88.6 kW. At 1.548 s, bus block 10 was energized by closing the circuit breaker of line 57-60.
3. IBDG 57 and 66 ramped up to 199.1 kW and 123.7 kW respectively. At 2.833 s, bus block 10 was energized by closing the circuit breaker of line 62-63.

The restoration of microgrid 4 completed in four stages and involved 3048 messages. The timeline of the four stages of restoration is given below:

1. At 0.571 s, bus block 14 was energized by closing the circuit breaker of diesel generator 76. At 1.041 s, bus block 15 was energized by closing the circuit breaker of line 76-77.
2. At 3.112 s, bus block 13 was energized by closing the circuit breaker of line 67-72.
3. IBDG 67, 81, 82, 101 and 105 ramped up to 175.9 kW, 109.5 kW, 107.5 kW, 91.3 kW and 90.0 kW respectively. Bus blocks 16, 17 and 19 were energized at 4.676 s, 5.532 s and 6.612 s respectively.
4. IBDG 67, 81, 82, 93, 95, 101 and 105 ramped up to 197.5 kW, 263.3 kW, 249.5 kW, 128.9 kW, 123.9 kW, 176.3 kW and 189.9 kW respectively. At 8.935 s, bus block 18 was energized by closing the circuit breaker of line 91-93. At 10.156 s, bus block 20 was energized by closing the circuit breaker of line 105-108.

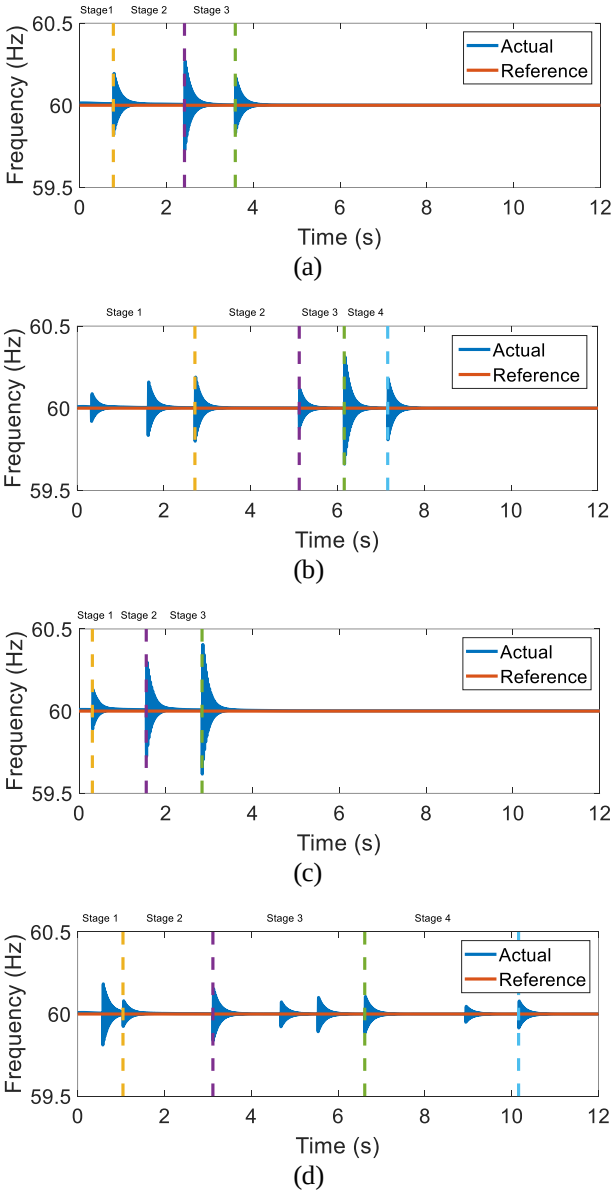

Figure 7: Frequency responses of diesel generators for four stages in case 1: (a) MG1 (b) MG2 (c) MG3 (d) MG4.

B. Case 2: Moderate communication network congestion.

Multi-agent coordination is very important for microgrid transient stability. Any coordination error between the microgrid controller and team agents can lead to serious consequences. Before switching additional load, sufficient spinning reserve must be available in the power system. This prevents over-stressing of the running generators. If any generator fails to start or ramp up at the correct time, the over-

stressed generators can lose synchronism. This can cause huge frequency swings and trigger the electrical protection system.

Moderate communication system congestion was simulated in case 2. This resulted in unexpected delay of generator control signals. As a result, additional bus blocks were energized before ramping up the incoming grid-following generators to the scheduled power reference. This caused the four grid-forming diesel generators to get overloaded as shown in Figure 8.

The restoration of microgrid 1 completed in two stages and involved 828 messages. The timeline of the two stages of restoration is given below:

1. IBDG 8 was commanded to ramp up to 815.4 kW. At 0.749 s, bus block 2 was energized by closing the circuit breakers of diesel generator 13 and IBDG 8.
2. A communication error occurred which caused the generator commands to be delayed. At 2.088 s, IBDG 1, 7 and 8 started ramping up to 132.8 kW, 131.7 kW and 844.0 kW respectively. Before the ramping was completed, bus block 1 and 3 were energized at 3.031 s and 3.427 s respectively.

The restoration of microgrid 2 completed in three stages and involved 2100 messages. The timeline of the three stages of restoration is given below:

1. IBDG 23 and 40 ramped up to 604.8 kW and 858.6 kW respectively. Bus blocks 4, 5 and 7 were energized at 0.304 s, 1.485 s and 2.466 s respectively.
2. A communication error occurred which caused the generator commands to be delayed. At 4.056 s, IBDGs 23, 40 and 47 started ramping up to 632.8 kW, 877.8 kW and 145.0 kW respectively. Before the ramping was completed, bus block 8 was energized by closing circuit breaker of line 42-44 at 5.647 s.
3. A communication error occurred which caused the generator commands to be delayed. At 7.490 s, IBDG 23, 29, 40, 47 and 51 started ramping up to 666.9 kW, 106.8 kW, 888.4 kW, 284.7 kW and 137.7 kW respectively. Before the ramping was completed, bus block 6 and 9 was energized at 9.031 s and 9.335 s respectively.

The restoration of microgrid 3 completed in three stages and involved 888 messages. The timeline of the three stages of restoration is given below:

1. At 0.294 s, bus block 11 was energized by closing the circuit breaker of diesel generator 60.
2. A communication error occurred which caused the generator commands to be delayed. At 1.373 s, IBDG 57 started ramping up to 76.4 kW. Before the ramping was completed, bus block 10 was energized by closing the circuit breaker of line 57-60 at 2.453 s.
3. A communication error occurred which caused the generator commands to be delayed. At 3.574 s, IBDG 57 and 66 started ramping up to 199.1 kW and 123.7 kW respectively. Before the ramping was completed, bus block 10 was energized by closing the circuit breaker of line 62-63 at 4.696 s.

The restoration of microgrid 4 completed in four stages and involved 3048 messages. The timeline of the four stages of restoration is given below:

1. At 0.527 s, bus block 14 was energized by closing the circuit breaker of diesel generator 76. At 0.942 s, bus block 15 was energized by closing the circuit breaker of line 76-77.
2. At 4.392 s, bus block 13 was energized by closing the circuit breaker of line 67-72. At 3.964 s, bus block 17 was energized by closing the circuit breaker of line 76-86.
3. A communication error occurred which caused the generator commands to be delayed. At 6.688 s, IBDG 67, 81, 82, 93, 95, 101 and 105 started ramping up to 138.2 kW, 107.3 kW, 106.6 kW, 112.3 kW, 106.5 kW, 85.6 kW and 92.8 kW respectively. Before the ramping was completed, bus block 16, 18 and 19 were energized at 7.822 s, 8.227 s and 8.986 s respectively.
4. A communication error occurred which caused the generator commands to be delayed. At 11.468 s, IBDG 67, 81, 82, 93, 95, 101, 105 and 108 started ramping up to 190.7 kW, 224.3 kW, 222.1 kW, 232.5 kW, 212.1 kW, 179.1 kW, 200.5 kW and 99.1 kW respectively. Before the ramping was completed, bus block 20 was energized by closing the circuit breaker of line 105-108 at 13.950 s.

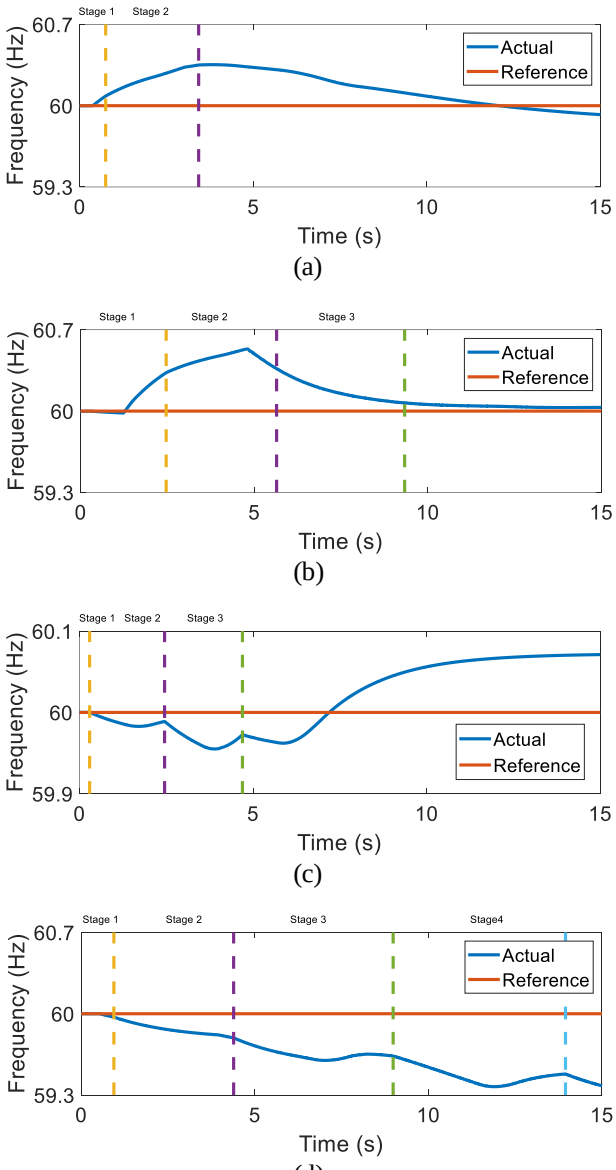

Figure 8: Frequency responses of diesel generators in case 2: (a) MG1 (b) MG2 (c) MG3 (d) MG4.

The unexpected delay in control of IBDG 1 can be seen in Figure 9. Switching additional loads before ramping up the generators caused the generators to lose stability. The grid forming synchronous generators quickly lost synchronism when they got over-stressed.

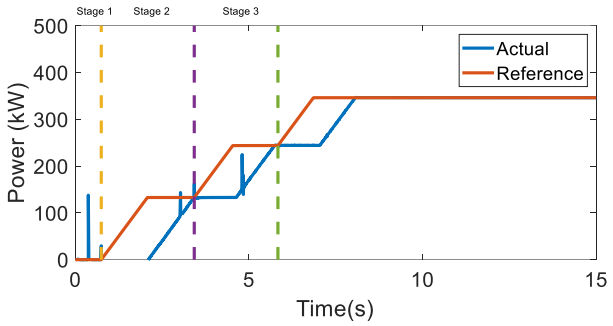

Figure 9: Difference between reference and actual active power of IBDG 1 due to communication error.

C. Case 3: Heavy communication network congestion.

Another simulation was carried out to analyze the impact of serious communication failure on microgrid stability. In case 3, heavy communication network congestion was simulated to analyze the importance of multi-agent coordination for microgrid stability. In order to simulate communication failure for each restoration stage, the DER control commands were executed after switching all the scheduled bus blocks. The resulting frequency variation of four grid-forming diesel generators is shown in Figure 10.

The restoration of microgrid 1 completed in two stages and involved 828 messages. The timeline of the two stages of restoration is given below:

1. IBDG 8 was commanded to ramp up to 815.4 kW. At 0.749 s, bus block 2 was energized by closing the circuit breakers of diesel generator 13 and IBDG 8.
2. A communication error occurred which caused the generator commands to be delayed. At 3.427 s, IBDG 1, 7 and 8 started ramping up to 132.8 kW, 131.7 kW and 844.0 kW respectively. Before the ramping was completed, bus block 1 and 3 were energized at 3.031 s and 3.427 s respectively.

The restoration of microgrid 2 completed in three stages and involved 2100 messages. The timeline of the three stages of restoration is given below:

1. IBDG 23 and 40 ramped up to 604.8 kW and 858.6 kW respectively. Bus blocks 4, 5 and 7 were energized at 0.304 s, 1.485 s and 2.466 s respectively.
2. A communication error occurred which caused the generator commands to be delayed. At 5.647 s, IBDGs 23, 40 and 47 started ramping up to 632.8 kW, 877.8 kW and 145.0 kW respectively. Before the ramping was completed, bus block 8 was energized by closing circuit breaker of line 42-44 at 5.647 s.
3. A communication error occurred which caused the generator commands to be delayed. At 9.335 s, IBDG 23, 29, 40, 47 and 51 started ramping up to 666.9 kW, 106.8 kW, 888.4 kW, 284.7 kW and 137.7 kW respectively. Before the ramping was completed, bus block 6 and 9 was energized at 9.031 s and 9.335 s respectively.

The restoration of microgrid 3 completed in three stages and involved 888 messages. The timeline of the three stages of restoration is given below:

1. At 0.294 s, bus block 11 was energized by closing the circuit breaker of diesel generator 60.
2. A communication error occurred which caused the generator commands to be delayed. At 2.453 s, IBDG 57 started ramping up to 76.4 kW. Before the ramping was completed, bus block 10 was energized by closing the circuit breaker of line 57-60 at 2.453 s.
3. A communication error occurred which caused the generator commands to be delayed. At 4.696 s, IBDG 57 and 66 started ramping up to 199.1 kW and 123.7 kW respectively. Before the ramping was completed, bus block 10 was energized by closing the circuit breaker of line 62-63 at 4.696 s.

The restoration of microgrid 4 completed in four stages and involved 3048 messages. The timeline of the four stages of restoration is given below:

1. At 0.527 s, bus block 14 was energized by closing the circuit breaker of diesel generator 76. At 0.942 s, bus block 15 was energized by closing the circuit breaker of line 76-77.
2. At 4.392 s, bus block 13 was energized by closing the circuit breaker of line 67-72. At 3.964 s, bus block 17 was energized by closing the circuit breaker of line 76-86.
3. A communication error occurred which caused the generator commands to be delayed. At 8.986 s, IBDG 67, 81, 82, 93, 95, 101 and 105 started ramping up to 138.2 kW, 107.3 kW, 106.6 kW, 112.3 kW, 106.5 kW, 85.6 kW and 92.8 kW respectively. Before the ramping was completed, bus block 16, 18 and 19 were energized at 7.822 s, 8.227 s and 8.986 s respectively.
4. A communication error occurred which caused the generator commands to be delayed. At 13.950 s, IBDG 67, 81, 82, 93, 95, 101, 105 and 108 started ramping up to 190.7 kW, 224.3 kW, 222.1 kW, 232.5 kW, 212.1 kW, 179.1 kW, 200.5 kW and 99.1 kW respectively. Before the ramping was completed, bus block 20 was energized by closing the circuit breaker of line 105-108 at 13.950 s.

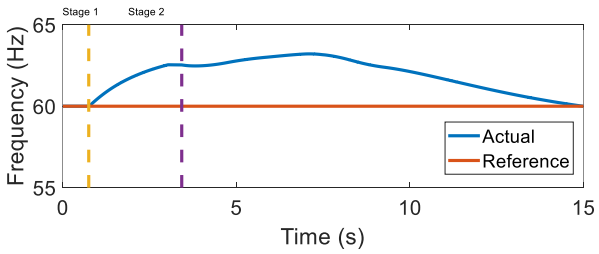

(a)

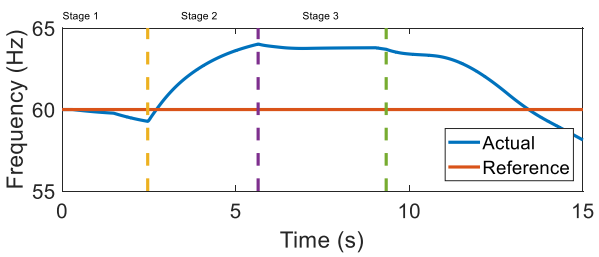

(b)

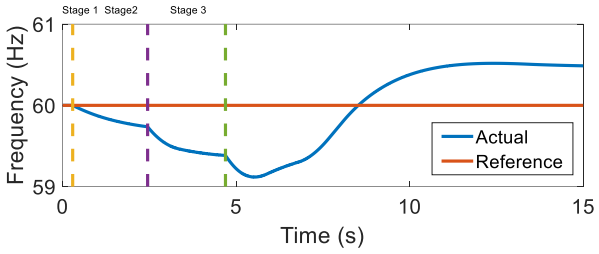

(c)

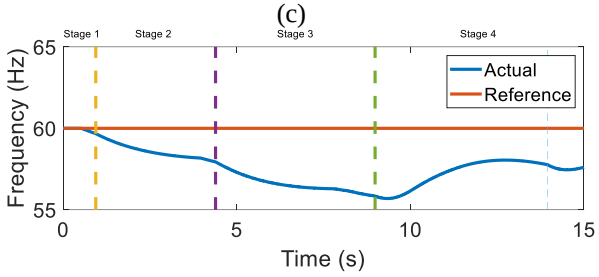

(d)

Figure 10: Frequency responses of diesel generators in case 3: (a) MG1 (b) MG2 (c) MG3 (d) MG4.

The unexpected delay in control of IBDG 1 can be seen in Figure 11. Switching additional loads before ramping up the generators caused the generators to lose stability. The grid forming synchronous generators quickly lost synchronism when they got over-stressed. Soon, the frequency swing exceeded the safe operation limit and the GridLAB-D Newton Raphson solver failed to converge to a solution [7].

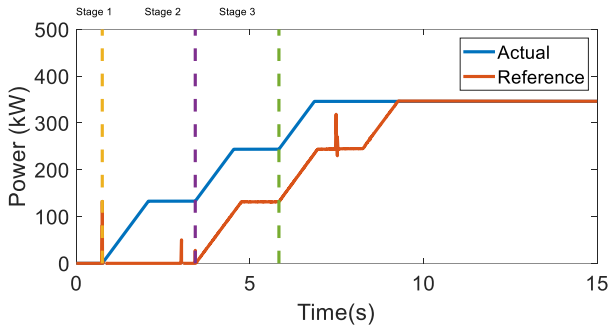

Figure 11: Difference between reference and actual real power of IBDG 1 due to communication error.

VI. Discussion

The transient fault records prove that the MISOCP optimization model does not capture the complete picture of the power system. It was incapable of forecasting the transient response of generators, transmission lines, and loads. As a result, the optimized restoration solution resulted in severe voltage, current, and frequency spikes. These transients can damage sensitive electronic equipment and trigger the electrical protection system.

Microgrid controllers used the measurements of distributed IEDs to quantify the damage afflicted on the generators. This transient response provided feedback for the next stage of the rolling horizon optimization. In effect, the dynamic feedback based on wide-area situational monitoring improved the restoration of inverter-dominated microgrids [1] [3].

The different subsystems operated cooperatively with two-way negotiations to exchange information and control signals. Perfect coordination was required between the DERs, smart switches and microgrid controller. Switching additional loads before ramping up the generators caused the running generators to lose stability. The grid forming synchronous generators quickly lost synchronism when they got over-stressed.

VII. Conclusion

This research demonstrated a cyber-physical implementation of a resilient distribution system. The proposed decentralized restoration strategy focused on formation of microgrids. The switching sequence determined by solving the MISOCP optimization problem was implemented over a distributed multi-agent control framework. The test results have demonstrated the importance of hard real-time communication in the control and management of smart grids. It was proved that communication failure between microgrid controller and remote controlled DERs was hazardous for the microgrid stability. Our future work on this research will focus on implementation of the MAS in a real-world application and testing the system in more complex scenarios.

References

[1] Q. Zhang, Z. Ma, Y. Zhu and Z. Wang, "A two-level simulation-assisted sequential distribution system restoration model with frequency dynamics constraints", IEEE Transactions on Smart Grid, vol. 12, no. 5, pp. 3835-3846, Sept. 2021.

[2] A. Sharma, D. Srinivasan and A. Trivedi, "A decentralized multiagent system approach for service restoration using DG islanding", in IEEE Transactions on Smart Grid, vol. 6, no. 6, pp. 2784-2793, 2015.

[3] M. Ghorbani, F. Mohammadi, M. Choudhry, A. Feliachi and D. Ashby, "Hardware design for distributed MAS-based fault location in power distribution systems", 2014 IEEE PES General Meeting Conference & Exposition, pp. 1-5, 2014.

[4] A. Sharma, W. Arokiasami and D. Srinivasan, "A multi-agent approach for service restoration with distributed generation", 2013 IEEE Innovative Smart Grid Technologies-Asia (ISGT Asia), pp. 1-6, 2013.

[5] A. Arif and Z. Wang, "Networked microgrids for service restoration in resilient distribution systems", in IET Generation, Transmission and Distribution, vol. 11 no. 14, pp. 3612-3619, 2017.

[6] A. Sharma, D. Srinivasan and A. Trivedi, "A decentralized multi-agent approach for service restoration in uncertain environment", in IEEE Transactions on Smart Grid, vol. 9, no. 4, pp. 3394-3405, 2018.

[7] D. Chassin, K. Schneider and C. Gerkensmeyer, "GridLAB-D: An open-source power systems modeling and simulation environment", 2008 IEEE/PES Transmission and Distribution Conference and Exposition, pp. 1-5, 2008.

[8] M. Ghorbani, M. Choudhry and A. Feliachi, "A multiagent design for power distribution systems automation", in IEEE Transactions on Smart Grid, vol. 7, no. 1, pp. 329-339, 2016.

[9] The NS3 network simulator. (https://www.nsnam.org).

[10] 123-Bus Feeder. [Online]. Available: https://site.ieee.org/pes-testfeeders/resources.